Inelastic light scattering and light emission from single and double wall carbon nanotubes

Yan Yin[1], Stephen Cronin[2], Andrew Walsh[1], Alexander Stolyarov[2], Michael Tinkham[2], Anthony Vamivakas[3], R.R Bacsa[4], SelimÜnlü[3,1], Bennett Goldberg[1,3], Anna Swan[3] and Wolfgang Bacsa[3,5]

[1]Physics department, Boston University, Boston, MA 02215
[2]Physics department, Harvard University, Cambridge, MA 02138,
[3]Electrical and Computer Engineering Department, Boston University, Boston, MA 02215
[4]Nanolab Inc**,** Newton, MA 02458
[5]LPST-IRSAMC CNRS, Université, Paul Sabatier, 31062 Toulouse, France; bacsa@lspt.ups-tlse.fr

ABSTRACT

We use inelastic light scattering (Raman) to probe individual and isolated single wall carbon nanotubes, suspended in air over trenches to explore the influence of the environment on the electronic transition energies. We find narrow and predominantly symmetric resonance profiles which are significantly downshifted as compared to isolated tubes in aqueous surfactant suspensions. A lower limit of the exciton binding energy in SWNTs is deduced by using the observed optical transition energies of SWNTs in SDS solutions. Photoluminescence is observed from narrow diameter double wall carbon nanotubes in aqueous surfactant suspensions.

Keywords: carbon nanotubes, optical transition energies, chirality, photoluminescence

1 INTRODUCTION

Carbon nanotubes are one dimensional model systems (1). The large one dimesional singularites in the electronic density of states lead to optical transitions which are sensitive to the chirality of the carbon nanotube. With the help of maps of the photoluminescence signal as a function of excitation energy from a distribution of single wall carbon nanotubes, in a surfactant suspension, it was possible to assign the emission peaks to a particular chirality (2). The assignment is based on comparing the distribution of emission peaks with the predicted distribution of values for all chiralities of semiconducting tubes using the tight binding model of graphene and applying the zone folding scheme. Although the theoretical values are significantly shifted to lower energies the correspondence of the distribution of photoluminescence peaks was sufficient to identify the tube chirality. It is believed that strong electron confinement in the tube leads to an increase of the electronic band gap and to the formation of excitons (3). This is in part consistent with the higher experimental observed energies of the photoluminescence peaks. The photoluminescence excitations studies have been carried out on tubes surrounded by surfactant molecules to isolate them and prevent any agglomeration which prevents any radiative recombination. But the surfactant itself is believed to influence the optical transition energies. In this context we have carried out experiments of individual and isolated single wall carbon nanotubes suspended over trenches to measure the intrinsic optical properties of SWNTs. Furthermore we have used inelastic light scattering as a function of excitation to map the energetic positions of the optical transition energies (tunable resonance Raman spectroscopy). This has the advantage that singularities in the electronic density of states can also be detected for metallic tubes apart of the fact that resonance Raman profiles are narrower than the photoluminescence emission bands due to the fundamental differences of the underlining physical process. Double wall carbon nanotubes are of interest due to the fact that the internal tube is protected from the interaction with its environment. We present here first photoluminescence spectra from double wall carbon nanotubes (DWNTs).

2 EXPERIMENTAL

The samples are prepared by first etching 1-1.5 μm wide trenches with markers in quartz substrates by reactive ion etching (RIE) in CF_4 plasma. SWNTs are grown over the trenches by chemical vapor deposition in methane gas at 900°C using a 1nm thick film of Fe as the growth catalyst (4). The tube concentration is lower than 1tube/ μm^2 as verified by scanning probe microscopy. A continuous wave tunable Ti-sapphire laser is used as the excitation laser source and we use a Renishaw RM1000B system with a motorized stage after custom-built modifications in order to achieve tunable Raman data collection for excitation wavelengths from 720 to 830*nm* (1.72 to 1.49*eV*). Filters are tuned by tilt and any beam offset is corrected by a matched filter tilt. The use of filters and a single grating offers a high through-put system and low signal to noise

ratios. A 600 g/mm grating is used, yielding ~2-3 cm^{-1} /pixel. The laser beam is focused by a 100X objective on a single nanotube which is suspended over the trench in air. The FWHM of the Gaussian spot-profile is 0.42 μm at E_{laser}=875 nm. 1-2 *mW* constant excitation laser power was used during a mapping. Measurements of Stokes and anti-Stokes intensity ratios show that no heating of the nanotubes takes place under such power density. We observe that the Raman signal from tubes on the substrate, are strongly suppressed. The entire collected signal originates therefore from the suspended part of the tube. Typical Stokes radial breathing mode (RBM) count rates are 3-35 counts/second. We map out the resonant excitation profile (REP) by changing the excitation wavelength. Each REP is measured twice with staggered 2 *nm* separation in excitation wavelength to check the repeatability.

3 RAMAN MAPPING

Figure 1 shows a Raman map of the radial breathing mode of one individual and isolated carbon nanotube using a step size of 0.5 μm (comparable to lateral resolution). The RBM frequencies are used to assign specific chiral indices (n,m) to the observed optical resonance. We observe that the Raman signal of the radial breathing mode is localized to the section where the tube crosses the trench. The trench location is indicated with two horizontal lines in figure 1.

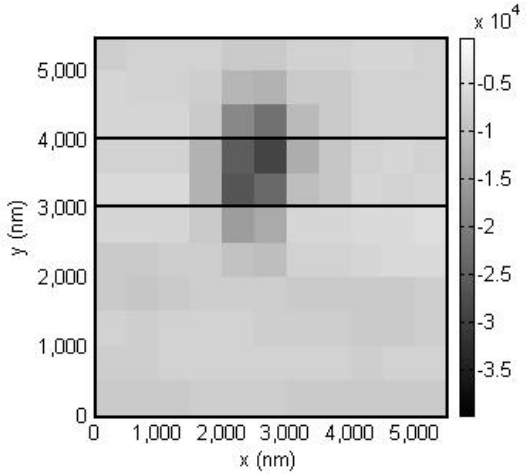

Figure 1 Spatial map of radial breathing mode intensity of one individual and isolated single wall carbon nanotube across a 1μm wide trench. Horizontal lines show the edge of the trench. Excitation wavelength: 798nm.

We attribute the disappearance of the Raman signal of the CNT to the interaction of the nanotube with the substrate and to local field variations. Incident and reflected waves are out of phase at the interface which leads to destructive interference and a reduction of the time averaged local field. The expected local field variation depends on the amplitude of the reflected wave.

Figure 2 shows a series of inelastic light spectra of the radial breathing mode for a fixed location on the nanotube by varying the excitation wavelength. The intensity of the radial breathing mode is enhanced as the excitation wavelength is in resonance with the one dimensional singularity of the tube. The radial breathing mode frequency is inversely proportional to the tube diameter and the observed resonance can then be related to the tube diameter. This can be repeated for individual and isolated tubes of different diameter to obtain a distribution of optical transition energies.

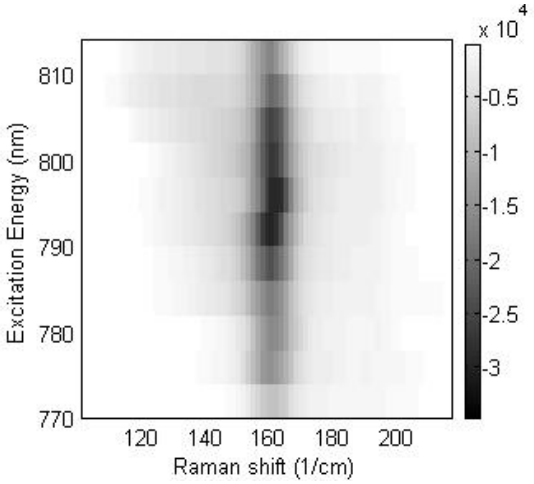

Figure 2 Spectra of radial breathing mode of individual and isolated SWNT as a function of laser excitation energy.

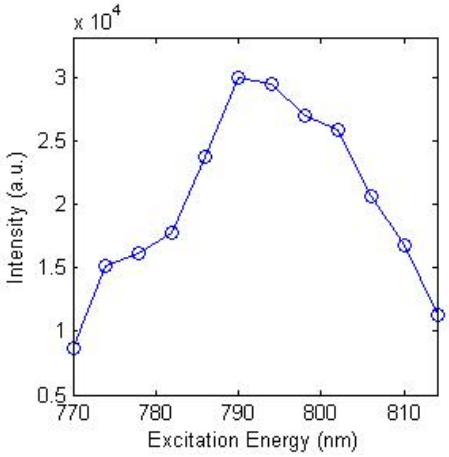

Figure 3 Resonance profile of radial breathing mode at 162cm^{-1} extracted from figure 2.

The resonance profile has contributions due to the resonant enhancement for the incoming and scattered light, separated by the addition of the phonon energy of the radial

breathing mode. The resonance profile is then fitted using the time-dependent, third-order perturbation theory for the Raman process in a one dimensional (1D) systems (5,6). We note that even though the van Hove singularities are asymmetric around the resonance, the resulting Raman intensity profile is symmetric (5).

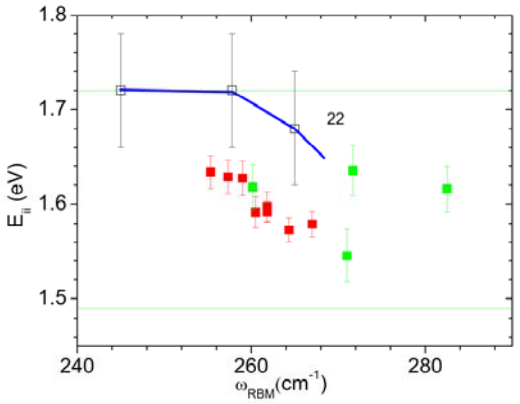

Figure 4 Measured E_{ii} vs. ω_{RBM} for the SWNTs measured by tunable RRS. The filled symbols are measured for SWNT suspended in air, squares denotes semiconducting tubes from RRS form tubes in SDS Ref [6, 7]. The numbers denote the 2n+m families. The energy ranges shown for each point are the spectral width.

The fitting determines the location of the E_{22} resonance energy and the spectral width η. The resonant profile has been recorded on a series of single and isolated SWNTs to determine the E_{22} and the corresponding width η. About half of the nanotubes have a η ranging from 8 to 18 meV and the remaining broadening parameters range up to 50 meV in decreasing numbers. The minimum η value we observed is 8.8 meV, similar to the only previously reported REP measurement of one single tube on a Si substrate (7). The tubes with wider resonance profile are believed to be affected by defects. The narrow broadening (~10 meV) measured for ~1/3 of the tubes is either a measure of the intrinsic lifetime broadening for a single suspended tube, or, possibly broadened by the finite suspension length (~1 μm) across the trench. The overall width of the resonance for the RBM REP can be estimated by $\eta+E_{phonon}$, ~ 25-50 meV. PLE measurements from a single tube suspended in air show a symmetric E^S_{22} excitation profile with a width of 44 meV, about 5 times broader than our REP data (8). This difference can be explained by the difference in the underlining physical process. In PL, absorption, intra- and inter-band phonon relaxation and emission rates all involves real states, where transition rates can be calculated by Fermi's golden rule (9). On the other hand resonance Raman scattering is described by third order time dependent perturbation theory with a three-step phase coherent quantum mechanical process resulting in scattered Raman signal. In either the incoming or outgoing resonance situation, it is necessary for the excited electron to scatter from a real to a virtual intermediate electronic state (or vice-versa). This explains the narrower resonance Raman profile. Figure 4 shows a systematic downshift (~100 *meV*), compared with SDS data. We find that the average line broadening η is ~14 meV for the isolated tubes suspended in air which is significantly narrower than for HiPCO tubes wrapped in SDS where the resonant peaks are broadened by 65 meV (10, 11) and 120 meV for bundles (11). These two observations show clearly the influence of the environment on optical transition energies.

Moore *et al* demonstrated that changing the surfactant can change the resonance energy by up to 25 meV (12). The resonance energies for bundles are found in between the reported SDS data and our data (11). The dielectric constant ε in a medium influence the interaction between electrons and holes, and as the dielectric constant increases, the electron hole-pair binding energy from the Coulomb attraction is screened. Perebinos *et al.* calculated the scaling of exciton binding energy for nanotubes embedded in a dielectric medium (13). They found a simple scaling relationship between the exciton binding energy and the dielectric constant, $E_b \propto R^{\alpha-2}\varepsilon^{-\alpha}$ for $4<\varepsilon<15$ where R is the tube radius and the scaling exponent, $\alpha=1.4$. Assuming an effective dielectric constant ε_{eff} for nanotubes in SDS, we can estimate the change in exciton binding energy with respect to a tube in air ($\varepsilon_{eff}=1$). Using $\alpha=1.4$ and $\varepsilon_{eff}^{SDS}\sim(1.5)^2$ one that E^{SDS}_b for a tube in SDS is only ~0.3 E^{air}_b, the binding energy for a tube in air. The observed shift of 0.1 eV, translates into a binding energy of ~0.15 eV provided the band edge energy position is not affected by the change in dielectric index which is much lower than expected. Spataru *et al* used an *ab initio* many-electron Green's function approach to calculate the exciton binding energy for an (8,0) tube, which was found to be $E_b^{8,0}\sim1$ eV. If we use this value and the scaling relationship for the radius (13) to estimate the binding energy for the (11, 0) zigzag tube in family 22, we obtain $E_b^{11,0} \sim E_b^{8,0}(R_{(8,0)}/R_{(11,0)})^{\alpha-2}\sim0.8$ eV, The difference of ~ 0.6 eV between our observed shift and the calculated binding energy could be taken as a measure of the shift of the band edge with dielectric constant, not accounted for in the scaling calculation.

3 PHOTOLUMINESCENCE FROM DOUBLE WALL CARBON NANOTUBES

Double wall carbon nanotubes (DWNTs) are of interest due to the fact that the internal tube is protected from

environmental effects and the intrinsic properties of internal carbon nanotubes are preserved. While photoluminescence have been observed by SWNTs in SDS, the solubility of DWNTs double in SDS is considerably lower and only very weak photoluminescence signals have been observed so far.

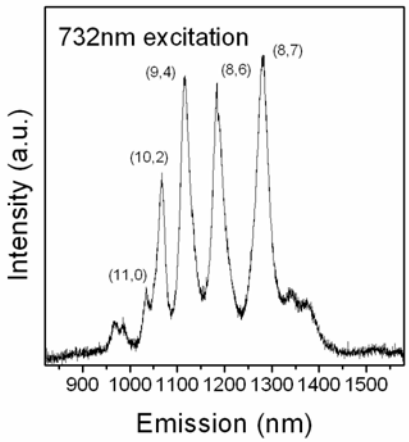

Figure 4 Photoluminescence spectrum of surfactant suspended double wall carbon nanotubes exited at 732nm.

By optimizing the surfactant, however, it is possible to improve the suspensions of double carbon nanotubes. Figure 4 shows the photoluminescence spectrum of a suspension of double wall carbon nanotubes excited at 732nm. We observe several emission bands where three of them are clearly split in doublets. DWNT samples contain also single and triple wall carbon nanotubes (<30%). We can attribute the observed the spectrum to tubes with more than one wall due to the fact that the surfactant is optimized for multiwall carbon nanotubes. The interaction of the two layers is expected to influence the emission spectrum. In general the chirality (helicity) of the two tubes is not commensurate and this opens the possibility that one or both of the two tubes are metallic or semiconducting. It is expected the tube-tube interaction depends on chirality. The interaction will be larger with metallic tubes and this could suppress any luminescence. This implies that the emission spectrum is broadened when measuring a distribution of tubes with different diameters. But we find that the experimental tube has in fact narrower spectral lines. This indicates that the tubes which do emit are in an environment which is more uniform or DWNTs have a higher relative quality. The observed emission spectrum can be compared to the photoluminescence spectrum of single wall carbon nanotubes. The emission bands are labeled with chiral indices using the assignment made for SWNTs in SDS.

4 CONCLUSION

We have observed individual and isolated SWNTs using tunable resonance Raman scattering to determine the optical transition energies. We are able to give a lower limit of the exciton binding energy in SWNTs by using the observed optical transition energies of SWNTs in SDS solutions. We find that photoluminescence spectra of double wall carbon nanotubes are strikingly similar to SWNTs in SDS.

REFERENCES

[1] S. Reich, C. Thomsen, J. Maultzsch, *Carbon Nanotubes* (Wiley-Vch 2004)

[2] Sergei M. Bachilo, Michael S. Strano, Carter Kittrell, Robert H. Hauge, Richard E. Smalley, and R. Bruce Weisman, *Science* **298**, 2361 (2002).

[3] T. Ando, J. Phys. Soc. Jpn. 66, 1066 (1996)

[4] J. Lefebvre, J. M. Fraser, Y. Homma, and P. Finnie, App. Phys. A **78**, p. 1107 (2004)

[5] R. M. Martin and L. M. Falicov, *Topics in Applied physics Vol 8 - Light scattering in solids I*, chapter 3, page 79 to page 95

[6] M. Canonico, G. B. Adams, C. Poweleit, J. Menéndez, J. B. Page, G. Harris, H. P. van der Meulen, J. M. Calleja, and J. Rubio, *Phys. Rev. B.* **65**, 201402(2002)

[7] A. Jorio, R. Saito, J. H. Hafner, C. M. Lieber, M. Hunter, T. McClure, G. Dresselhaus, and M. S. Dresselhaus, *Phys. Rev. Lett.* **86**, 1118 (2001).

[8] J. Lefebvre, J. M. Fraser, Y. Homma, P. Finnie, *Phys. Rev. B* **69**, 075403, (2004)

[9] J. Jiang, R. Saito, A. Grüneis, S. G. Chou, Ge. G. Samsonidze, A. Jorio, G. Dresselhaus and M. S. Dresselhaus. *Phys. Rev. B* **71**, 045417 (2005)

[10] H. Telg, J. Maultzsch, S. Reich, F. Hennrich, and C. Thomsen, *Phys. Rev. Lett.* **93**, 177401(2004).

[11] C. Fantini, A. Jorio, M. Souza, M. S. Strano, M. S. Dresselhaus, and M. A. Pimenta, *Phys. Rev. Lett.* **93**, 147406 (2004)

[12] V. C. Moore, M. S. Strano, E. H. Haroz, R. H. Hauge, R.E. Smalley Nano Lett. 3, 1379, (2003)

[13] Perebinos, J. Tersoff and Ph Avouris. *Phys. Rev. Lett.* **93** (2004)